International Journal of Heat and Technology
Vol. 40, No. 2, April, 2022, pp. 619-626
Journal homepage: http://iieta.org/journals/ijht

Dynamic Characteristics Analysis of Tri-Stable Cantilever Piezoelectric Energy Harvester with a Novel-type Dynamic Amplifier

Dawei Man[1,2*], Huaiming Xu[1], Gaozheng Xu[1], Deheng Xu[1], Liping Tang[1,2], Qinghu Xu[1,2]

[1] School of Civil Engineering, Anhui Jianzhu University, Hefei 230601, China
[2] BIM Engineering Center of Anhui Province, Hefei 230601, China

Corresponding Author Email: mandawei@ahjzu.edu.cn

https://doi.org/10.18280/ijht.400232

Received: 6 January 2022
Accepted: 15 March 2022

Keywords:
piezoelectric energy harvester, novel-type dynamic magnifier, harmonic balance method, dynamic features

ABSTRACT

In this paper, a non-linear tri-stable piezoelectric cantilever energy harvester with a novel-type dynamic magnifier was proposed to achieve more effective broadband energy harvesting under low-level ambient excitations. According to the generalized Hamilton principle, a mathematical distributed parameter model of the piezoelectric energy harvester was proposed. The novel-type dynamic magnifier is a system consisting of two spring masses, one placed between the fixed end of the piezoelectric beam and the L-shaped frame, and the other, between the L-shaped frame and the base. The harmonic balance method was adopted to work out the analytical expressions of the steady-state displacement, steady-state output voltage and power amplitude of the energy harvester system. The effects of the distance between the magnets, the spring stiffness of the dynamic magnifier, and the load resistance on the performance of the system were also investigated. The results show that different from that of the conventional tri-stable piezoelectric energy harvester, the frequency response curve of the proposed novel-type energy harvester system with a two-spring-mass dynamic magnifier exhibits two peaks as a result of the interactions of the coupled elastic system, where the left peak stands for the resonant value of the tri-stable piezoelectric energy harvester, while the right one the resonant value of the dynamic magnifier. It is able to achieve higher output power over a broader frequency band under low-level environmental excitations, and the harvested power can be significantly strengthened if the mass and stiffness of the dynamic magnifier are selected properly.

1. INTRODUCTION

In recent years, with the wide use of wireless sensor networks in such fields as architectural structures and health surveillance, powering wireless sensor networks with energy harvested from the surrounding environment has become quite promising. Piezoelectric energy harvesters (PEHs) are able to collect vibrational energy from the ambient environment and transform it into long-lasting and clean electrical energy. What is more, PEHs have simple and compact structures that are easy to integrate and have great potential for self-powering wireless sensor nodes [1, 2]. In the early days, scholars tended to focus on the research of linear PEHs. However, the operating frequency band of conventional linear PEHs is very narrow, and high energy capture efficiency can be realized only when the external excitation frequency is close to the intrinsic frequency of the system [3-6]. The non-linear effect enables piezoelectric energy harvesting over a wider frequency band. Since the operating bandwidth is increased, non-linear PEHs show lower sensitivity to variations in external excitation frequencies than linear ones and are more applicable in the acquisition of energy from environmental vibrations in actual practice. Bi-stable, tri-stable and multi-stable energy harvesters with magnetic interactions are all commonly used non-linear PEHs [7, 8]. A non-linear bi-stable piezoelectric energy harvester (BPEH) can oscillate between two potential wells and produce high output power under sufficient external excitation. Stanton et al. [9, 10] built an analysis model for BPEH composed of permanent magnets and a piezoelectric cantilever beam, and studied the dynamic features of the system by numerical simulation and experimental methods. Tang et al. [11] studied the voltage output of a bi-stable piezoelectric cantilever energy harvester system when the excitations are different, and discussed the effect of magnet spacing on the response of the system. Compared with those of the linear PEH, the operating bandwidth and output power of the non-linear BPEH have been significantly increased after entering the inter-well motion. However, the BPEH cannot break through the potential barrier under weak ambient vibration, which greatly reduces the output performance of the system [12-15].

In order to increase the efficiency of energy harvesting by PEHs in a weak excitation environment, Zhou et al. [16] established a non-linear tri-stable piezoelectric energy harvester (TPEH) on the basis of the magnetic bi-stable piezoelectric cantilever model. Under the circumstance where there is an appropriate distance and angle between two fixed magnets, the system's potential energy function will exhibit three stable states and the potential wells will be shallower and wider than that for BPEH. Kim and Seok [17] and Kim et al. [18] investigated a TPEH that has rotatable magnets, and proved the energy capture advantage of this TPEH in a wide operating frequency band. Li et al. [19] demonstrated the outstanding energy capture performance of a TPEH for

random excitations through numerical simulation and tests. Zhou and Zuo [20] and Ma et al. [21] designed an asymmetric TPEH which can enter the inter-well motion easily and output higher power under low-level excitations, and they also discovered that, compared with system parameters, the harvester is more sensitive to external excitations. In the above studies, BPEH and TPEH were fixed on rigid bases. If the environmental excitations are at a very low level, the rigid base directly excited by these environment excitations will not be able to produce sufficient kinetic energy to make TPEH break through the potential barriers.

In light of the above problems of BPEHs and TPEHs, Wang et al. [22, 23] proposed a configuration that includes an elastic amplifier for amplifying the basel excitations so that it will produce enough kinetic energy to break through the potential well barriers and enter the large amplitude bi-stable inter-well motion, thus leading to higher power generation. In this paper, a novel-type TPEH with two dynamic magnifiers (TDM) was proposed. In light of the size effect of the tip magnet, the distributed parameter electro-mechanical coupling equation of the TPEH with two dynamic magnifiers (TPEH+TDM) was constructed according to the generalized Hamilton principle, and the analytical solution of the energy harvester system was derived with the harmonic balance method. The influences of the distance between the magnets, the mass and eccentricity of the tip magnet, the load resistance, the stiffness of the dynamic magnifier on the dynamic performances of the energy harvester system were also investigated.

2. MATHEMATICAL MODEL OF TPEH+TDM

The diagram of the TPEH+TDM proposed in this paper is shown in Figure 1. The piezoelectric energy harvester system consists of a TPEH with two dynamic magnifiers. The TPEH contains a piezoelectric cantilever beam with a tip magnet (represented by A) and two external magnets (represented by B and C) fixed at the right wall of the L-shaped frame. The cantilever beam has a substrate layer, whose two surfaces are covered by two identical thin piezoelectric layers (PZTs). The two PZTs have opposite polarities in the thickness direction and are connected electrically in series with an equivalent load resistance (represented by R). The TDM comprises two dynamic magnifiers (denoted as DM1 and DM2), where DM1 consists of a spring k_b and a L-shaped mass block, which are mechanically connected in series, while DM2 is basically a spring (k_f)-mass (M_f) system located between the fixed end of the cantilever beam and the bottom of the L-shaped mass block. The horizontal gap between the tip magnet and the external magnet is d_h, and the vertical one from the tip magnet to magnet B is d_v. l and b represent the length and width of the cantilever beam, respectively; h_s and t_p are the thickness of the substrate layer and the PZTs, respectively; e denotes the eccentricity of the tip magnet.

$v_m(t)$ and $v_b(t)$ denote the vibration displacement of DM1 and the base, respectively; s stands for the coordinate along the neutral axis of the cantilever beam; and $v(s, t)$ denote the displacement of the cantilever beam at position s relative to its fixed end. The constitutive equations of the piezoelectric cantilever beam are given as follows:

$$\left.\begin{aligned} T_1^s &= Y_s S_1^s \\ T_1^p &= Y_p\left(S_1^p - d_{31}E_3\right) \\ D_3 &= d_{31}T_1 + \varepsilon_{33}^T E_3 \end{aligned}\right\} \tag{1}$$

where, Y is Young's modulus; subscript/superscript p and s stand for the PZTs and the substrate layer; S_1 and T_1 denote the strain and the stress of the cantilever beam, respectively; D_3 represents the electric displacement; d_{31} and ε_{33}^T are the piezoelectric constant and dielectric constant, respectively; and $E_3 = -V(t)/(2t_p)$ is the electric field, where V(t) represents the voltage. The strain produced in the piezoelectric cantilever beam can be written as $S_1^s = S_1^p = -yv''$.

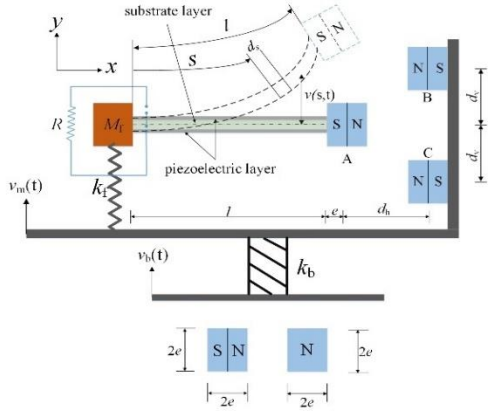

Figure 1. Diagram of the proposed TPEH+TDM

The generalized Hamilton's principle of the TPEH+TDM system is described as follows:

$$\int_{t_1}^{t_2}\left[\delta\left(T_k + W_e - U_e - U_m - U_d\right) + \delta W\right]dt = 0 \tag{2}$$

where, T_k, W_e, U_e, U_m, U_d and W stand for the kinetic energy, electrical energy, strain energy, magnetic potential energy and elastic potential of the dynamic magnifiers and the external work, respectively. T_k, W_e, U_e and U_d can be defined as:

$$\begin{aligned} T_k = {} & \frac{1}{2}\int_0^l m\left(\dot{v} + \dot{v}_m(t)\right)^2 ds + \\ & \frac{1}{2}M_t\left(\dot{v}(l,t) + e\dot{v}'(l,t) + \dot{v}_m(t)\right)^2 + \frac{1}{2}J\dot{v}'(l,t)^2 \\ & + \frac{1}{2}M_f\left(\dot{v}(0,t) + \dot{v}_m(t)\right)^2 + \frac{1}{2}M_m\dot{v}_m(t)^2 \end{aligned} \tag{3}$$

$$W_e = \frac{1}{2}Y_p b d_{31}\left(h + \frac{t_p}{2}\right)V(t)\int_0^l v''ds + bl\varepsilon_{33}^S\frac{V(t)^2}{4t_p} \tag{4}$$

$$U_e = \frac{1}{2}\int_0^l\left[YIv''^2 - Y_p b d_{31}(h + \frac{t_p}{2})V(t)v''\right]ds \tag{5}$$

$$U_d = \frac{1}{2}k_f v(0,t)^2 + \frac{1}{2}k_b {v_m}^2 \tag{6}$$

where, $m = 2\rho_p t_p b + \rho_s h_s b$, in which ρ_p and ρ_s are the density of the PZTs and the substrate layer, respectively; M_t and J denote the mass and the rotary inertia of the tip magnet; ε_{33}^s is the permittivity. $h = \frac{h_s}{2}$, $YI = \frac{2}{3}\left[Y_s b h^3 + Y_p b\left(3h^2 t_p + 3h{t_p}^2 + {t_p}^3\right)\right]$.

According to our published work [24] and taking into account the eccentricity of the tip magnet, U_m can be expressed as follows:

$$
\begin{aligned}
U_{\mathrm{m}} = & \frac{\mu_0 M_{\mathrm{A}} V_{\mathrm{A}} M_{\mathrm{B}} V_{\mathrm{B}} \left\{ -\left(v(l,t) + \frac{ev'(l,t)}{\sqrt{1+v'(l,t)^2}} - d_{\mathrm{v}} \right)^2 + 2\left[d_{\mathrm{h}} + e\left(1 - \frac{1}{\sqrt{1+v'(l,t)^2}} \right) \right]^2 - 3\left[d_{\mathrm{h}} + e\left(1 - \frac{1}{\sqrt{1+v'(l,t)^2}} \right) \right] \right.}{4\pi\sqrt{1+v'(l,t)^2} \left\{ \left[d_{\mathrm{h}} + e\left(1 - \frac{1}{\sqrt{1+v'(l,t)^2}} \right) \right]^2 + \left(v(l,t) + \frac{ev'(l,t)}{\sqrt{1+v'(l,t)^2}} - d_{\mathrm{v}} \right)^2 \right\}^{5/2}} \\
& \left. \left(v(l,t) + \frac{ev'(l,t)}{\sqrt{1+v'(l,t)^2}} - d_{\mathrm{v}} \right) v'(l,t) \right\} \\
& + \frac{\mu_0 M_{\mathrm{A}} V_{\mathrm{A}} M_{\mathrm{B}} V_{\mathrm{B}} \left\{ -\left(v(l,t) + \frac{ev'(l,t)}{\sqrt{1+v'(l,t)^2}} + d_{\mathrm{v}} \right)^2 + 2\left[d_{\mathrm{h}} + e\left(1 - \frac{1}{\sqrt{1+v'(l,t)^2}} \right) \right]^2 - 3\left[d_{\mathrm{h}} + e\left(1 - \frac{1}{\sqrt{1+v'(l,t)^2}} \right) \right] \right.}{4\pi\sqrt{1+v'(l,t)^2} \left\{ \left[d_{\mathrm{h}} + e\left(1 - \frac{1}{\sqrt{1+v'(l,t)^2}} \right) \right]^2 + \left(v(l,t) + \frac{ev'(l,t)}{\sqrt{1+v'(l,t)^2}} + d_{\mathrm{v}} \right)^2 \right\}^{5/2}} \\
& \left. \left(v(l,t) + \frac{ev'(l,t)}{\sqrt{1+v'(l,t)^2}} + d_{\mathrm{v}} \right) v'(l,t) \right\}
\end{aligned} \tag{7}
$$

where, $\mu_0 = 4\pi \times 10^{-7} H \cdot m^{-1}$ is the magnetic permeability constant; M_{A} (M_{B} or M_C) and V_{A} (V_{B} or V_C) are the magnetization intensity and volume of the magnet A (B or C), respectively.

Using the Galerkin approach, $v(s, t)$ is assumed as:

$$
v(s,t) = \phi_r(s)\eta_r(t) \tag{8}
$$

where, $\varphi_r(s)$ and $\eta_r(t)$ represent respectively the R-order mode function and the generalized mode coordinates of the beam.

The mode function meets the orthogonal relations as below:

$$
\begin{aligned}
& \int_0^l \varphi_s(s) m \varphi_r(s) ds + \varphi_s(l) M_t \varphi_r(l) \\
& + \varphi_s(l) M_t e \varphi_r'(l) + \varphi_s(0) M_f \varphi_r(0) \\
& + \varphi_s'(l)(J + M_t e^2) \varphi_r'(l) \\
& + \varphi_s'(l) M_t e \varphi_r(l) = \delta_{rs}
\end{aligned} \tag{9}
$$

$$
\begin{aligned}
& \int_0^l \frac{\mathrm{d}^2 \varphi_s(s)}{\mathrm{d}s^2} YI \frac{\mathrm{d}^2 \varphi_r(s)}{\mathrm{d}s^2} \mathrm{d}s \\
& + \varphi_s(0) k_{\mathrm{f}} \varphi_r(0) = \omega_r{}^2 \delta_{rs}
\end{aligned} \tag{10}
$$

where, δ_{rs} represents the Kronecker delta. For the r-th mode, the resonance frequency is defined as $\omega_r = \lambda_r{}^2 \sqrt{YI/(ml^4)}$. The calculation process of the eigenvalue λ_r is described in literature [6].

Substitute Eq. (8) into Eq. (7), and then there is the Taylor's expansion of U_m at $\eta(t)$=0, which is expressed as:

$$
\begin{aligned}
U_{\mathrm{m}} = & k_0 - \frac{1}{2} k_1 \eta_1{}^2 \\
& + \frac{1}{4} k_2 \eta_1{}^4 + \frac{1}{6} k_3 \eta_1{}^6 + o(\eta_1{}^7)
\end{aligned} \tag{11}
$$

where, $k_0 = \dfrac{2\kappa q_1}{\left(d_{\mathrm{h}}{}^2 + d_{\mathrm{v}}{}^2\right)^2}$,

$$
k_1 = \frac{4\kappa}{\left(d_{\mathrm{h}}{}^2 + d_{\mathrm{v}}{}^2\right)^{5/2}} \left[q_1\left(2.5q_2 - 17.5q_3{}^2\right) - 5q_3 q_4\left(d_{\mathrm{h}}{}^2 + d_{\mathrm{v}}{}^2\right) - q_5 \right],
$$

$$
\begin{aligned}
k_2 = & \frac{8\kappa}{\left(d_{\mathrm{h}}{}^2 + d_{\mathrm{v}}{}^2\right)^{5/2}} \left[q_1\left(-2.5q_6 - 17.5q_3 q_7 + 4.38q_2{}^2 \right.\right. \\
& - 78.75q_2 q_3{}^2 + 144.375q_3{}^4\left.\right) \\
& + q_4\left(-2.5q_7 - 17.5q_2 q_3 + 52.5q_3{}^3\right)\left(d_{\mathrm{h}}{}^2 + d_{\mathrm{v}}{}^2\right) \\
& \left. q_5\left(-2.5q_2 + 17.5q_3{}^2\right) + 5q_3 q_8 + q_9 \right],
\end{aligned}
$$

$$
\begin{aligned}
k_3 = & \frac{12\kappa}{\left(d_h{}^2 + d_v{}^2\right)^{5/2}} [q_1(-2.5q_{10} + 13.125q_3 q_{11} + \\
& 8.75q_2 q_6 + 4.375q_7{}^2 - 78.78q_3{}^2 q_6 + \\
& 78.25q_2 q_3 q_7 - 288.75q_3{}^3 q_7 + 216.55q_2{}^2 q_3{}^2 - \\
& 6.56q_2{}^3 - 938.44q_2 q_3{}^4 + 938.44q_3{}^6) + \\
& q_4(1.875q_{11} - 17.5q_3 q_6 + 8.75q_2 q_7 - \\
& 78.75q_3{}^2 q_7 + 39.38q_2{}^2 q_3 - 288.75q_2 q_3{}^2 + \\
& 375.375q_3{}^5) + q_5(-2.5q_6 - 17.5q_3 q_7 + \\
& 4.375q_2{}^2 - 78.75q_2 q_3{}^2 144.375q_3{}^4) + \\
& q_8(-2.5q_7 - 17.5q_2 q_3 + 52.5q_3{}^3) + q_9(-2.5q_2 + \\
& 17.5q_3{}^2) + 5q_3 q_{12} + q_{13}],
\end{aligned}
$$

For the expressions of the coefficients κ and $q_{i=1\ldots13}$, please see the appendix.

The external virtual work can be written as:

$$
\begin{aligned}
\delta W = & \delta v_m \ddot{v}_b \left(M_m + M_t + ml + M_f \right) \\
& + \delta\eta(t) \ddot{v}_b \left(M_t \varphi_1(l) \right. \\
& + m \int_0^l \varphi_1(s) ds + M_t e \varphi_1'(l) \\
& \left. + M_f \varphi_1(0) \right)
\end{aligned} \tag{12}
$$

With Eq. (8) substituted into Eq. (2), considering only the first order mode, Lagrange's equation for the TPEH+TDM system is expressed as follows:

$$\begin{cases} \dfrac{\mathrm{d}}{\mathrm{d}t}\left(\dfrac{\partial L}{\partial \dot{v}_{\mathrm{m}}}\right)-\dfrac{\partial L}{\partial v_{\mathrm{m}}}+\dfrac{\partial W}{\partial v_{\mathrm{m}}}=0 \\ \dfrac{\mathrm{d}}{\mathrm{d}t}\left(\dfrac{\partial L}{\partial \dot{\eta}}\right)-\dfrac{\partial L}{\partial \eta}+\dfrac{\partial W}{\partial \eta}=F(t) \\ \dfrac{\mathrm{d}}{\mathrm{d}t}\left(\dfrac{\partial L}{\partial \dot{V}}\right)-\dfrac{\partial L}{\partial V}+\dfrac{\partial W}{\partial V}=Q(t) \end{cases} \tag{13}$$

where, $F(t)=-2\xi_1\omega_1\dot{\eta}_1(t)$ is the generalized dissipative force; ξ_1 is the damping ratio; $Q(t)=V(t)/R$ is the generalized output charge.

The electro-mechanical coupling equations of the TPEH+TDM system can be derived from Eq. (13):

$$\begin{cases} M_0\ddot{\eta}_1(t)+M_1\ddot{v}_m(t) \\ \quad +k_b v_m=-M_1\ddot{v}_b(t) \\ \ddot{\eta}_1(t)+2\xi_1\omega_1\dot{\eta}_1(t)+{\omega_1}^2\eta_1(t)-k_1\eta_1(t) \\ +k_2\eta_1(t)^3+k_3\eta_1(t)^5-\theta_1 V(t) \\ \quad +M_0\ddot{v}_m(t)=-M_0\ddot{v}_b(t) \\ C_p\dot{V}(t)+\dfrac{V(t)}{R}+\theta_1\dot{\eta}_1(t)=0 \end{cases} \tag{14}$$

where, $M_0=m\int_0^l\phi_1(s)ds+M_t\phi_1(l)+M_te\phi_1'(l)+M_f\phi_1(0)$, $M_1=ml+M_t+M_f+M_m$, ${\omega_1}^2=YI\int_0^l\phi_1''(s)^2ds+k_f\phi_1(0)^2$, $\theta_1=Y_pbd_{31}\left(h+\frac{t_p}{2}\right)\int_0^l\phi_1''(s)\,ds$, $C_p=\frac{bl\varepsilon_{33}^S}{2t_p}$.

where, $\omega_1^2=YI\int_0^l\varphi_1''ds, g_0=mg\int_0^l\varphi_1(s)ds+M_tg\varphi_1(l)$, $\Gamma_1=m\int_0^l\varphi_1(s)ds+M_t(\varphi_1(l)+e\varphi_1'(l))$, $\theta_1=Y_pbd_{31}(h+(t_p/2))\int_0^l\varphi_1(s)ds$, and $C_p=bl\varepsilon_{33}^S/2t_p$.

The excitation acceleration is defined as $\ddot{v}_b(t)=\bar{v}_b\cos(\omega_e t)$, where $\bar{v}_b$ is the excitation amplitude, ω_e the circular frequency, and C_{p} the capacitance. With the dimensionless parameters $x=\eta_1/l$, $V_m=v_m/l$, $V_b=v_b/l$, $\bar{V}=\frac{VC_p}{l\theta_1}$ and $\tau=\omega_1 t$ introduced, Eq. (14) can be rewritten as Eq. (15) in the dimensionless form.

$$\begin{cases} \dfrac{M_1-{M_0}^2}{K_b}x^{(4)}+\dfrac{2M_1\xi_1}{K_b}x^{(3)} \\ +\dfrac{M_1(1-K_1)+K_b}{K_b}\ddot{x}+2\xi_1\dot{x} \\ +(1-K_1)x+K_2x^3+K_3x^5 \\ +\dfrac{M_1K_2}{K_b}(6x\dot{x}^2+3x^2\ddot{x}) \\ +\dfrac{M_1K_3}{K_b}(20x^3\dot{x}^2+5x^4\ddot{x}) \\ -\dfrac{M_1\Theta}{K_b}\ddot{\bar{V}}-\Theta\bar{V}=F\cos(\omega\tau) \\ \dot{\bar{V}}+\alpha\bar{V}+\dot{x}=0 \end{cases} \tag{15}$$

where, $K_b=\frac{k_b}{{\omega_1}^2}$, $K_1=\frac{k_1}{{\omega_1}^2}$, $K_2=\frac{k_2l^2}{{\omega_1}^2}$, $\Theta=\frac{{\theta_1}^2}{C_p{\omega_1}^2}$, $\alpha=\frac{1}{C_pR_L\omega_1}$, $F=-\frac{M_0\bar{v}_b}{{\omega_1}^2l}$.

3. HARMONIC BALANCE ANALYSIS

The solution to Eq. (15) is assumed as:

$$\begin{cases} x=A(\tau)\sin(\omega\tau)+B(\tau)\cos(\omega\tau) \\ \bar{V}=C(\tau)\sin(\omega\tau)+D(\tau)\cos(\omega\tau) \end{cases} \tag{16}$$

where, A, B, C and D are undetermined coefficients, so the displacement amplitude of the cantilever beam can be represented as $a=\sqrt{A^2+B^2}$, and the output voltage amplitude can be expressed as $u=\sqrt{C^2+D^2}$.

Substitute Eq. (16) into (15) and let the constant terms on both sides of the equation and the coefficients of $sin(\omega\tau)$ and $cos(\omega\tau)$ be consistent. With higher harmonic terms and partial zero terms, the following equations are obtained:

$$Z_1\left(\ddot{A}-2\omega\dot{B}\right)+2\xi_1\dot{A}+Z_2B+Z_3A+Z_4C=0 \tag{17.1}$$

$$\begin{aligned} &Z_1\left(\ddot{B}-2\omega\dot{A}\right)+2\xi_1\dot{B}+Z_3B \\ &-Z_2A+Z_4D-F=0 \end{aligned} \tag{17.2}$$

$$\dot{C}-\omega D+\alpha C+\dot{A}-\omega B=0 \tag{17.3}$$

$$\dot{D}+\omega C+\alpha D+\dot{B}+\omega A=0 \tag{17.4}$$

where,

$$Z_1=\frac{K_1M_1+K_{\mathrm{b}}}{K_{\mathrm{b}}}$$

$$Z_2=\frac{2\xi_1M_1}{K_{\mathrm{b}}}\omega^3-2\xi_1\omega$$

,

$$Z_3=\frac{M_1-{M_0}^2}{K_b}\omega^4-\frac{(1-K_1)M_1+K_b}{K_b}\omega^2+1-K_1+\frac{3}{4}K_2a^2+\frac{5}{8}K_3a^4-\frac{3}{4}\frac{K_2M_1}{K_b}\omega^2a^2-\frac{5}{8}\frac{K_3M_1}{K_b}\omega^4a^4,$$

$$Z_4=\frac{\Theta M_1}{K_{\mathrm{b}}}\omega^2-\Theta$$

It is assumed that all the time derivatives of Eq. (17) are zero in the steady-state dynamics. Therefore, the displacement amplitude and the voltage amplitude can be calculated as follows:

$$a^2\left[\begin{array}{l}\left(Z_2+Z_4\dfrac{\alpha\omega}{\omega^2+\alpha^2}\right)^2 \\ +\left(Z_3-Z_4\dfrac{\omega^2}{\omega^2+\alpha^2}\right)^2\end{array}\right]=F^2 \tag{18}$$

Use Eq. (18) to calculate the steady-state displacement response amplitude a. Then, the steady-state output voltage amplitude and output power amplitude can be expressed as below:

$$u=\left(\frac{\omega}{\sqrt{\omega_2+\alpha^2}}\right)a \tag{19}$$

$$P = \frac{l^2 \theta_1^2 u^2}{C_p^2 R} \tag{20}$$

4. RESULTS AND DISCUSSION

This section investigates the effects of the magnet spacing, the mass and eccentricity of the tip magnet, the load resistance and the base dynamic magnifier on the dynamic features of the BPEH+TDM system. The geometric and material attributes are as follows:

$$l = 75\text{mm},\ b = 20\text{mm},\ h_s = 0.2\text{mm},$$
$$Y_s = 70\text{Gpa},\ \rho_s = 2700\text{kg/m}^3$$
$$M_t = 10 \times 10^{-3}\text{kg},\ M_m = 0.18\text{kg},$$
$$M_f = 16.5 \times 10^{-3}\text{kg},$$
$$M_A = M_B = M_C = 1.22 \times 10^6\ \text{A/m},$$
$$V_A = V_B = V_C = 1 \times 10^{-6}\text{m}^3,\ \xi_1 = 0.01,$$
$$Y_p = 60.98\text{Gpa},\ \rho_s = 7750\text{kg/m}^3,$$
$$d_{31} = -1.71 \times 10^{-10}\text{C/N},$$
$$\varepsilon_{33}^s = 1.33 \times 10^{-8}\text{F/m}.$$

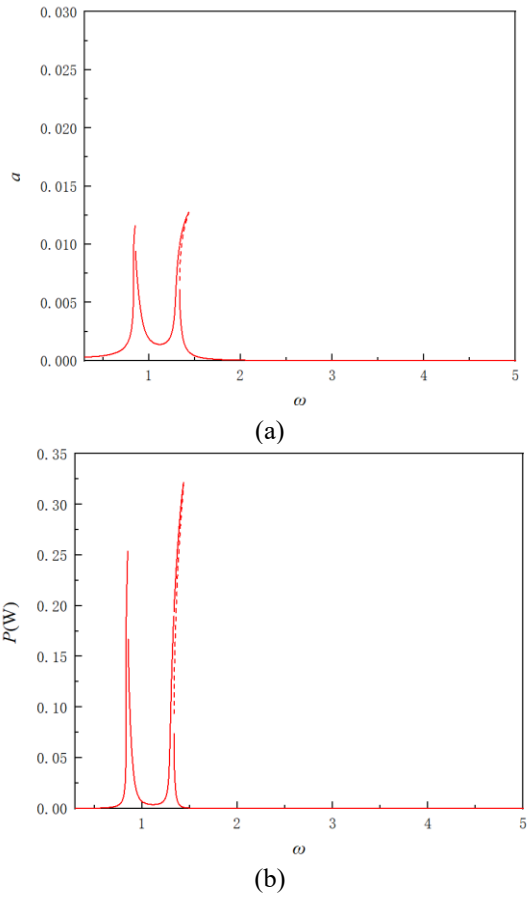

Figure 2. (a) Displacement amplitude, and (b) output power frequency response curve when e=0

Figures 2, 3 and 4 display the displacement and output power frequency response curves with different eccentricities of the tip magnet when d_v=8mm, d_h=21mm, k_f=15000, k_b=12000, M_t=10g and M_f=16.5g. It can be seen that there are two peaks in the frequency response curve, as a result of the interactions of the coupled elastic system, of which, the left peak stands for the resonant value of the TPEH, while the right one the resonant value of the dynamic magnifier. When e is 0 and 2.5 mm respectively, the corresponding displacement and power amplitude are very close. When e is set as 5mm, the system produces large inter-well motion, and the displacement and power in the left peak area increase significantly. The "right peak" area moves to the high frequency band with the increase of e.

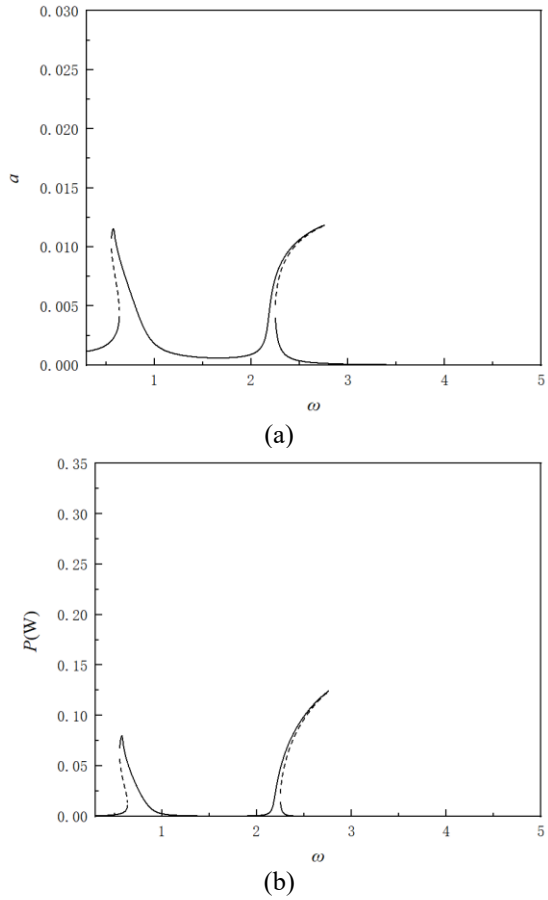

Figure 3. (a) Displacement amplitude and (b) output power frequency response curve when e=2.5mm

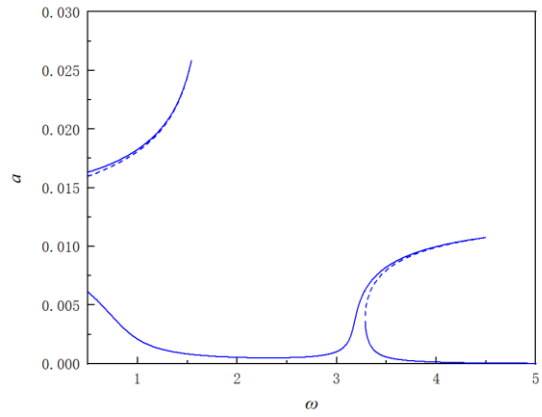

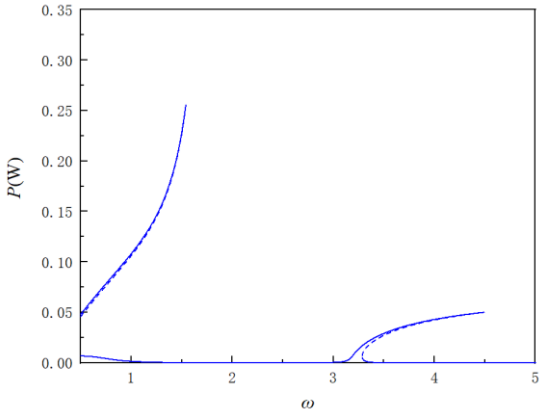

(b)

Figure 4. (a) Displacement amplitude and (b) output power frequency response curve when e=5mm

Figure 5 shows the variations in displacement and output power versus excited frequency with different values of d_h when d_v=8mm, k_f=15000, k_b=12000, e=0.0050, M_t=10g, M_f=16.5g. Figure 5 shows, as d_h increases, the peak displacement, peak power and band width in the "left peak" area of the system change very little, while those in the "right peak" area increase significantly. In addition, the "right peak" area shifts to the lower frequency band as d_h increases.

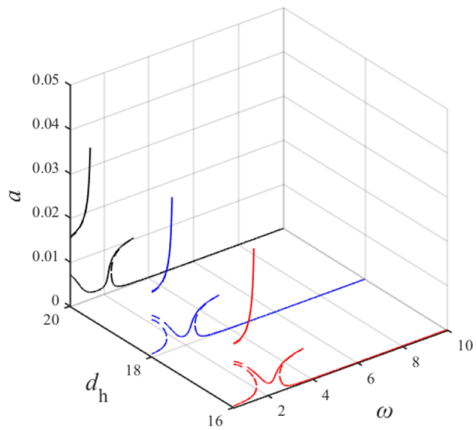

(a)

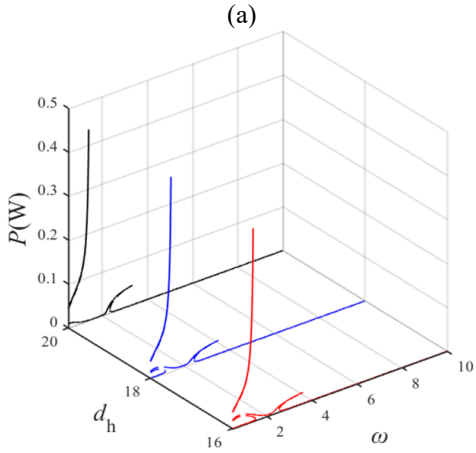

(b)

Figure 5. (a) Displacement amplitude and (b) output power frequency response curve with different values of d_h

The displacement and power frequency response curves with different values of M_t when d_v=8mm, d_h=21mm, k_f=15000, k_b=12000, e=0.0050, M_t=10g and M_f=16.5g are given in Figures 6. It shows that with the increase of M_t, the peak displacement and peak output power in the "left peak" area increase significantly, while those in the "right peak" area change very little. However, the bandwidth of the system is not sensitive to the increase of M_t.

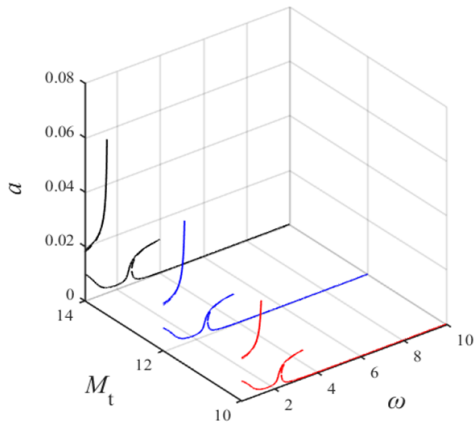

(a)

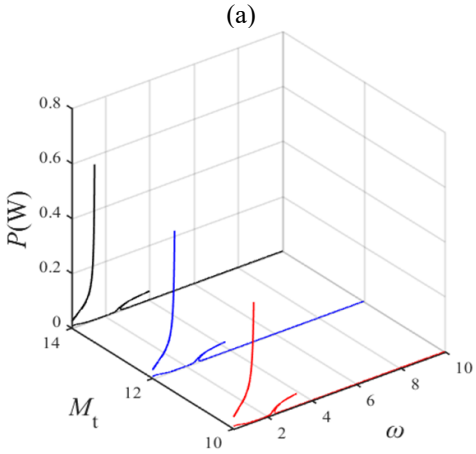

(b)

Figure 6. (a) Displacement amplitude and (b) output power frequency response curve with different values of M_t

Figure 7 shows the displacement and output power frequency response curves with different values of K_b when d_v=8mm, d_h=20mm, k_f=15000, k_b=12000, e=0.0050, M_t=10g, and M_f=16.5g. Figure 4 shows that reducing K_b can greatly improve the peak displacement and peak power in the "left peak" area, while the interwell motion displacement amplitude and output power amplitude change little in the "right peak" area. It can also be found that the "right peak" area shifts to the higher frequency band as K_b increases.

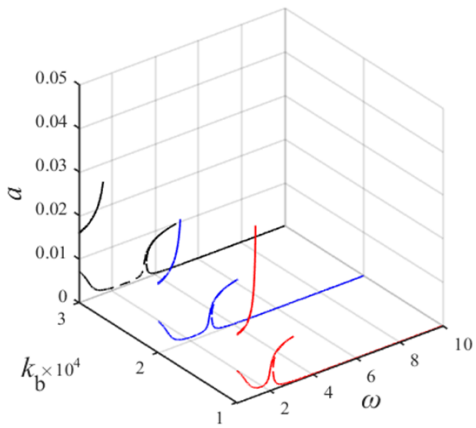

(a)

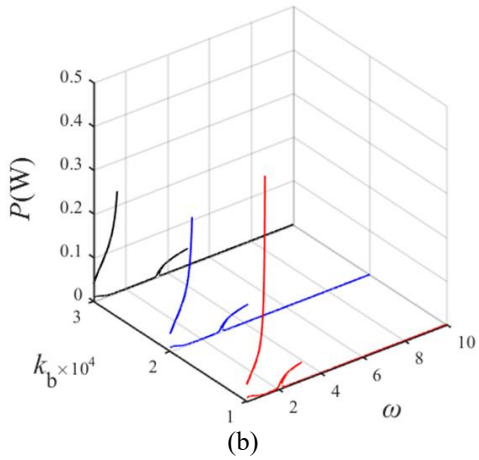

(b)

Figure 7. (a) Displacement amplitude and (b) output power frequency response curve with different values of k_b

Figure 8 shows the peak power variation curve with load resistance R for the system with different values of k_b when d_v=8mm, d_h=20mm, k_f=70000, e=0.0050, M_t=10g and M_f=16.5g. The results show that for a certain k_b, with the increase of R, the peak power of the system increases significantly (and reaches the first maximum value of peak power, corresponding to the local optimal load resistance of R_{opt1}), then decreases to a slight extent. After that, it increases again (and reaches the second maximum value of peak power, corresponding to the local optimal load resistance of R_{opt2}), and starts to gradually decrease.

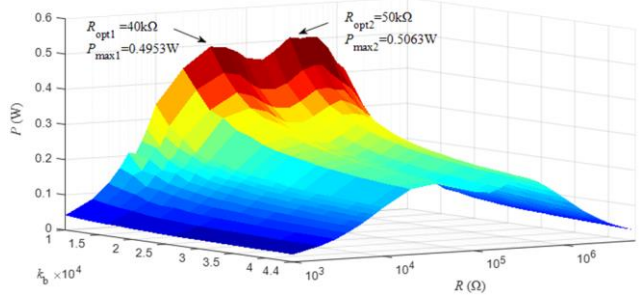

Figure 8. Peak power curves along with resistance changes under different values of k_b

5. CONCLUSIONS

This paper presented a theoretical framework for analysis and prediction of the dynamic responses of a TPEH+TDM system for the purpose of optimizing and improving the energy harvesting performance under low-level excitations. It also investigated the influences of magnet spacing, the stiffness of the base dynamic magnifier, the load resistance and the mass and eccentricity of the tip magnet on the TPEH+TDM system, with the following conclusions drawn.

(1) There are two peaks in the frequency response curve of the TPEH+TDM system as a result of the interactions of the coupled elastic system, where the left peak stands for the resonant value of the TPEH, while the right one, the resonant value of the dynamic magnifier.

(2) Increasing dh can increase the displacement and output power in the "right peak" area. and the "right peak" area moves towards the lower frequency band as dh increases.

(3) Reducing the stiffness of the base dynamic magnifier or increasing the mass of the tip magnet can significantly increase the peak displacement and peak power in the "left peak" area.

There are two local optimal resistances to make the peak output power of the system maximized, and the local optimal resistance increases as Kb increases, and at the same time, the corresponding peak output power also increases.

ACKNOWLEDGMENT

This research was funded by the Doctoral Startup Foundation of Anhui Jianzhu University (Grant No.: 2020QDZ07), the Project of Science and Technology Plan of Department of Housing and Urban-Rural Development of Anhui Province (Grant No.: 2020-YF15), the Anhui Provincial Natural Science Foundation (Grant No.: 2108085MA28).

REFERENCES

[1] Safaei, M., Sodano, H.A., Anton, S.R. (2019). A review of energy harvesting using piezoelectric materials: State-of-the-art a decade later (2008–2018). Smart Materials and Structures, 28(11): 113001.

[2] Tian, W., Ling, Z., Yu, W., Shi, J. (2018). A review of MEMS scale piezoelectric energy harvester. Applied Sciences, 8(4): 645. https://doi.org/10.3390/app8040645

[3] Sodano, H.A., Park, G., Inman, D.J. (2004). Estimation of electric charge output for piezoelectric energy harvesting. Strain, 40(2): 49-58. https://doi.org/10.1111/j.1475-1305.2004.00120.x

[4] Dutoit, N.E., Wardle, B.L., Kim, S.G. (2005). Design considerations for MEMS-scale piezoelectric mechanical vibration energy harvesters. Integrated Ferroelectrics, 71(1): 121-160. https://doi.org/10.1080/10584580590964574

[5] DuToit, N.E., Wardle, B.L. (2007). Experimental verification of models for microfabricated piezoelectric vibration energy harvesters. AIAA journal, 45(5): 1126-1137. https://doi.org/10.2514/1.25047

[6] Tang, L., Wang, J. (2017). Size effect of tip mass on performance of cantilevered piezoelectric energy harvester with a dynamic magnifier. Acta Mechanica, 228(11): 3997-4015. https://doi.org/10.1007/s00707-017-1910-8

[7] Zhou, S., Lallart, M., Erturk, A. (2022). Multistable vibration energy harvesters: Principle, progress, and perspectives. Journal of Sound and Vibration, 528: 116886. https://doi.org/10.1016/j.jsv.2022.116886

[8] Erturk, A., Inman, D.J. (2011). Piezoelectric Energy Harvesting. John Wiley & Sons.

[9] Stanton, S.C., McGehee, C.C., Mann, B.P. (2010). Nonlinear dynamics for broadband energy harvesting: Investigation of a bistable piezoelectric inertial generator. Physica D: Nonlinear Phenomena, 239(10): 640-653. https://doi.org/10.1016/j.physd.2010.01.019

[10] Stanton, S.C., Owens, B.A., Mann, B.P. (2012). Harmonic balance analysis of the bistable piezoelectric inertial generator. Journal of Sound and Vibration, 331(15): 3617-3627. https://doi.org/10.1016/j.jsv.2012.03.012

[11] Tang, L., Yang, Y., Soh, C.K. (2012). Improving functionality of vibration energy harvesters using

magnets. Journal of Intelligent Material Systems and Structures, 23(13): 1433-1449. https://doi.org/10.1177/1045389X12443016
[12] Jung, J., Kim, P., Lee, J.I., Seok, J. (2015). Nonlinear dynamic and energetic characteristics of piezoelectric energy harvester with two rotatable external magnets. International Journal of Mechanical Sciences, 92: 206-222. https://doi.org/10.1016/j.ijmecsci.2014.12.015
[13] Hosseinloo, A.H., Turitsyn, K. (2015). Non-resonant energy harvesting via an adaptive bistable potential. Smart Materials and Structures, 25(1): 015010. https://doi.org/10.1088/0964-1726/25/1/015010
[14] Fang, Z.W., Zhang, Y.W., Li, X., Ding, H., Chen, L.Q. (2018). Complexification-averaging analysis on a giant magnetostrictive harvester integrated with a nonlinear energy sink. Journal of Vibration and Acoustics, 140(2): 021009. https://doi.org/10.1115/1.4038033
[15] Erturk, A., Inman, D.J. (2011). Broadband piezoelectric power generation on high-energy orbits of the bistable Duffing oscillator with electromechanical coupling. Journal of Sound and Vibration, 330(10): 2339-2353. https://doi.org/10.1016/j.jsv.2010.11.018
[16] Zhou, S., Cao, J., Inman, D.J., Lin, J., Li, D. (2016). Harmonic balance analysis of nonlinear tristable energy harvesters for performance enhancement. Journal of Sound and Vibration, 373: 223-235. https://doi.org/10.1016/j.jsv.2016.03.017
[17] Kim, P., Seok, J. (2015). Dynamic and energetic characteristics of a tri-stable magnetopiezoelastic energy harvester. Mechanism and Machine Theory, 94: 41-63. https://doi.org/10.1016/j.mechmachtheory.2015.08.002
[18] Kim, P., Son, D., Seok, J. (2016). Triple-well potential with a uniform depth: Advantageous aspects in designing a multi-stable energy harvester. Applied Physics Letters, 108(24): 243902. https://doi.org/10.1063/1.4954169
[19] Li, H.T., Qin, W.Y., Lan, C.B., Deng, W.Z., Zhou, Z.Y. (2015). Dynamics and coherence resonance of tri-stable energy harvesting system. Smart Materials and Structures, 25(1): 015001. https://doi.org/10.1088/0964-1726/25/1/015001
[20] Zhou, S., Zuo, L. (2018). Nonlinear dynamic analysis of asymmetric tristable energy harvesters for enhanced energy harvesting. Communications in Nonlinear Science and Numerical Simulation, 61: 271-284. https://doi.org/10.1016/j.cnsns.2018.02.017
[21] Ma, X., Li, H., Zhou, S., Yang, Z., Litak, G. (2022). Characterizing nonlinear characteristics of asymmetric tristable energy harvesters. Mechanical Systems and Signal Processing, 168: 108612. https://doi.org/10.1016/j.ymssp.2021.108612
[22] Wang, G., Liao, W.H., Yang, B., Wang, X., Xu, W., Li, X. (2018). Dynamic and energetic characteristics of a bistable piezoelectric vibration energy harvester with an elastic magnifier. Mechanical Systems and Signal Processing, 105: 427-446. https://doi.org/10.1016/j.ymssp.2017.12.025
[23] Wang, G., Ju, Y., Liao, W.H., Zhao, Z., Li, Y., Tan, J. (2021). A hybrid piezoelectric device combining a tri-stable energy harvester with an elastic base for low-orbit vibration energy harvesting enhancement. Smart Materials and Structures, 30(7): 075028. https://doi.org/10.1088/1361-665X/ac057b
[24] Man, D., Xu, D., Kuang, X., Kang, X., Xu, Q., Zhang, Y. (2021). Analysis of dynamic characteristics of tristable piezoelectric energy harvester based on the modified model. Mathematical Problems in Engineering, 2021: 3832406. https://doi.org/10.1155/2021/3832406

APPENDIX

$$\kappa = \mu M_{\mathrm{A}} V_{\mathrm{A}} M_{\mathrm{B}} V_B / 4\pi = \mu M_{\mathrm{A}} V_{\mathrm{A}} M_{\mathrm{C}} V_C / 4\pi,$$

$$q_1 = 2d_{\mathrm{h}}{}^2 - d_{\mathrm{v}}{}^2,$$

$$q_2 = \begin{pmatrix} d_{\mathrm{h}} e\varphi_1'(l)^2 + e^2\varphi_1'(l)^2 \\ +2e\varphi_1(l)\varphi_1'(l) + \varphi_1(l)^2 \end{pmatrix} / \left(d_{\mathrm{h}}{}^2 + d_{\mathrm{v}}{}^2\right),$$

$$q_3 = d_{\mathrm{v}}\left(e\phi_1'(l) + \phi_1(l)\right) / \left(d_{\mathrm{h}}{}^2 + d_{\mathrm{v}}{}^2\right),$$

$$q_4 = 2d_{\mathrm{v}} \begin{bmatrix} \left(e\varphi_1'(l) + \varphi_1(l)\right) \\ +3d_h d_{\mathrm{v}} \varphi_1'(l) \end{bmatrix} / \left(d_{\mathrm{h}}{}^2 + d_{\mathrm{v}}{}^2\right),$$

$$q_5 = -0.5\left(2d_{\mathrm{h}}{}^2 - d_{\mathrm{v}}{}^2\right)\varphi_1'(l)^2 - \left(e\varphi_1'(l) + \varphi_1(l)\right)^2 - d_h e\varphi_1'(l)^2 - 3d_{\mathrm{h}}\varphi_1(l)\varphi_1'(l),$$

$$q_6 = \begin{pmatrix} -0.75d_{\mathrm{h}} e\varphi_1'(l)^4 - 0.75e^2\varphi_1'(l)^4 \\ -e\varphi_1(l)\varphi_1'(l)^3 \end{pmatrix} / \left(d_{\mathrm{h}}{}^2 + d_{\mathrm{v}}{}^2\right),$$

$$q_7 = d_{\mathrm{v}} e\phi_1'(l)^3 / \left(d_{\mathrm{h}}{}^2 + d_{\mathrm{v}}{}^2\right),$$

$$q_8 = -0.5 \begin{bmatrix} 2d_{\mathrm{v}}\left(e\varphi_1'(l) + \varphi_1(l)\right) \\ +3d_{\mathrm{h}} d_{\mathrm{v}} \varphi_1'(l) \end{bmatrix} \varphi_1'(l)^2 + 0.5d_{\mathrm{v}} e\varphi_1'(l)^3,$$

$$q_9 = -0.375\left(2d_{\mathrm{h}}{}^2 - d_{\mathrm{v}}{}^2\right)\varphi_1'(l)^4 - \left[-\left(e\varphi_1'(l) + \varphi_1(l)\right)^2 + 2d_{\mathrm{h}} e\varphi_1'(l)^2 - 3d_{\mathrm{h}}\left(e\varphi_1'(l) + \varphi_1(l)\right)\varphi_1'(l)\right]\varphi_1'(l)^2 - 0.5e\varphi_1(l)\varphi_1'(l)^3,$$

$$q_{10} = \begin{pmatrix} 0.625d_{\mathrm{h}} e\varphi_1'(l)^6 + 0.625e^2\varphi_1'(l)^6 \\ +0.75e\varphi_1(l)\varphi_1'(l)^5 \end{pmatrix} / \left(d_{\mathrm{h}}{}^2 + d_{\mathrm{v}}{}^2\right),$$

$$q_{11} = d_{\mathrm{v}} e\phi_1'(l)^5 / \left(d_{\mathrm{h}}{}^2 + d_{\mathrm{v}}{}^2\right),$$

$$q_{12} = -0.375 \begin{bmatrix} 2d_{\mathrm{v}}\left(e\varphi_1'(l) + \varphi_1(l)\right) \\ +3d_{\mathrm{h}} d_{\mathrm{v}} \varphi_1'(l) \end{bmatrix} \varphi_1'(l)^4 - 0.625d_{\mathrm{v}} e\varphi_1'(l)^5$$

$$q_{13} = -0.313\left(2d_{\mathrm{h}}{}^2 - d_{\mathrm{v}}{}^2\right)\varphi_1'(l)^6 - 0.25e^2\varphi_1'(l)^6 - 0.75e\varphi_1(l)\varphi_1'(l)^2 - 0.375\varphi_1(l)^2\varphi_1'(l)^4 - 0.25d_{\mathrm{h}} e\varphi_1'(l)^6 - 1.125d_{\mathrm{h}}\varphi_1(l)\varphi_1'(l)^5 - 0.125e\varphi_1(l)\varphi_1'(l)^5.$$